Phase-matching and Peak Nonlinearity Enhanced Third-Harmonic Generation in Graphene Plasmonic Coupler

Tingting Wu,[1,2] Yu Luo,[1,*] Stefan A. Maier,[3,4] and Lei Wei[1,2,†]

[1]*School of Electrical and Electronic Engineering, Nanyang Technological University, 50 Nanyang Avenue, 639798 Singapore*
[2]*CINTRA CNRS/NTU/THALES, UMI 3288, Research Techno Plaza, 50 Nanyang Drive, 637553 Singapore*
[3]*The Blackett Laboratory, Department of Physics, Imperial College London, London SW7 2AZ, UK*
[4]*Nanoninstitut München, Fakultät für Physik, Ludwig-Maximilians-Universität München, 80539 München, Germany*

Strong nonlinear optical effects generally require giant optical fields interacting with the nonlinear media. Doped graphene hosts electrically tunable plasmons with long lifetimes that interact strongly with light. We investigate a graphene plasmonic coupler and explore two mechanisms to pursue highly efficient third-harmonic generation (THG): (1) phase matching of graphene plasmons at fundamental- and third-harmonic frequencies and (2) peak third-order nonlinear susceptibility of doped graphene. The third-harmonic wave is mainly converted from the evanescent mode of the incident light and the THG efficiency is found to be enhanced by over 10 orders of magnitude compared with a bare monolayer graphene. The significantly enhanced nonlinear optical responses in the graphene plasmonic coupler make this configuration an ideal platform for the development of alternative frequency generators and for signal processing at midinfrared and terahertz frequencies.

I. INTRODUCTION

Third-harmonic generation (THG) due to light concentration in nanoscale volumes has various applications in nanomedicine [1], photocatalysis [2], and biosensing [3]. Under illumination at frequency ω, the third-order nonlinear susceptibility ($\chi^{(3)}$) induces a polarizability $P_3 = \varepsilon_0 \chi^{(3)} E_1 E_1 E_1$, with E_1 being the electric field at the fundamental frequency (FF). The overall THG conversion efficiency depends on the overlap between the fundamental- and third-harmonic (TH) modes. The efficiency of the THG process is low due to two major limitations, i.e., small $\chi^{(3)}$ and phase mismatch between the FF and the induced TH waves [4,5]. Thus, to achieve more efficient nonlinear conversion, promising solutions are to either enhance the electromagnetic field intensity to compensate the small $\chi^{(3)}$ or to overcome the phase mismatch along the nonlinear propagation [6–9].

Plasmonic nanostructures have been widely explored to alleviate the small nonlinear response in the traditional process owing to their large light enhancement at tiny geometrical features. THG efficiency as high as 0.45% in the

near-infrared regime has been achieved [10]. However, this mechanism is not applicable in midinfrared and terahertz frequencies. Doped graphene has been proposed as an alternative promising candidate for nonlinear plasmons as it sustains electrically tunable optical excitations with long lifetimes and high-electric-field enhancement at infrared and terahertz regimes [11,12]. Graphene plasmons actually provide higher light confinement with lower loss compared with metallic plasmons [13,14]. For practical applications, three major techniques have been proposed to excite graphene plasmons [12,15,16]. Furthermore, recent third-harmonic generation [17–21] and four-wave mixing [22,23] have confirmed the strong nonlinear responses in undoped, plasmons-free graphene. Specifically, graphene exhibits an intriguing merit for THG by a resonant peak in $\chi^{(3)}$ at a frequency of two-thirds of its Fermi level (E_F) [24].

We explore here the combination of phase-matching and resonant three-photon transition in a graphene plasmonic coupler to achieve highly efficient THG. Under a phase-matching condition (PMC), the FF and TH waves propagate with the same phase velocity, and accordingly, the TH-signal energy accumulates continuously along its propagation. PMC can be realized by purely modulating the surrounding dielectric permittivity of the graphene plasmonic coupler. This procedure also helps in tuning the

_____
[*]luoyu@ntu.edu.sg
[†]wei.lei@ntu.edu.sg

resonant peak $\chi^{(3)}$ of doped graphene to further enhance the THG conversion.

II. PLASMONIC COUPLER STRUCTURE

Figure 1(a) illustrates the three-dimensional (3D) configuration of the proposed graphene plasmonic coupler where the FF beam at ω incidents from the left graphene nanoribbon [labeled a in Fig. 1(b)] and a TH wave at 3ω is generated from the other side [labeled b in Fig. 1(b)]. The two-dimensional (2D) cross section is shown in Fig. 1(b). During the third-order nonlinear process, the excited pump plasmons in a nanoribbon act as the nonlinear transformer that converts the guided-evanescent-mode energy to the stimulated TH mode in nanoribbon b. Graphene sections with a fixed Fermi level of $E_{F0} = 1$ eV are taken as background states possessing little contribution to the THG. $\epsilon_1 = 2$ and $\epsilon_2 = 1$ are the permittivities of the nondispersive silica substrate and the surrounding air. ϵ_3 is to be determined to obtain the PMC. The fixed background Fermi level of 1 eV aims to increase the evanescent mode component, while the small distance C of 2 nm between the two graphene nanoribbons enables a strong coupling between the two propagating modes, thus increasing the pump-harmonic-mode overlap for efficient THG.

III. RESULTS AND DISCUSSION

We use coupled-mode theory [25] to model the power transfer between the FF and TH waves. The nonlinear polarizability is modeled as a source term. Only the Kerr nonlinearity is considered and the THG conversion efficiency is evaluated by $\eta = P_{\text{TH}}/P_0$. P_{TH} stands for the highest produced TH power and P_0 stands for the initial FF power. The propagation distance required to reach the maximum TH power is taken as the interaction length. Under phase-matching and lossless conditions, the generated TH intensity I_3 in a bulk sample from an incident beam with irradiance I_1 can be described

by: $I_3 = \frac{(3\omega)^2 (2\pi)^4}{n_3 n_1^3 c^4} |\chi^{(3)}|^2 I_1^3 L^2 \rho^2$ [26]. n_1 and n_3 are the refractive indices of the nonlinear matter at FF and TH frequencies, L is the interaction length, and ρ is the pump-harmonic spatial overlap. This TH intensity expression indicates the crucial roles of third-order nonlinear susceptibility and pump-harmonic spatial overlap for efficient THG.

To characterize the THG conversion with plasmonic wave propagation along the graphene coupler, we investigate two main properties. First, the PMC, which represents the ideal state where the FF power continuously transfers to the TH power. Second, the peak $\chi^{(3)}$ of the doped graphene. We use COMSOL to obtain the effective mode index and the corresponding mode profiles at FF and TH plasmonic waves, respectively (see Appendix A). The complex permittivity of graphene is modeled by the Kubo formula, which accounts for the intraband and interband electron transitions [27,28]. The nonlinear conductivity (which is 17 orders of magnitude smaller than the linear conductivity) is not considered during the calculation. For a single graphene sheet surrounded by two dielectric media with permittivities of ϵ_1 and ϵ_2, the dispersion relation of the guided surface plasmons is modeled by [29] $\frac{\epsilon_1}{\sqrt{\beta^2 - \epsilon_1 \omega^2/c^2}} + \frac{\epsilon_2}{\sqrt{\beta^2 - \epsilon_2 \omega^2/c^2}} = j \frac{\sigma(\omega)}{\omega \epsilon_0}$, where β is the propagation constant of the guided mode, ω is the angular frequency, c is the free-space light speed, $\sigma(\omega)$ is the graphene conductivity, and ϵ_0 is the vacuum permittivity. The effective mode index is defined as $\text{Re}(\beta)/k_0$, where k_0 is the corresponding wavenumber in free space. Modifying the permittivity of the surrounding dielectric medium will change the plasmonic wavevector. This suggests phase matching between the FF and TH plasmonic modes in the graphene plasmonic coupler through tuning the surrounding permittivity.

For a thin graphene layer, since the thickness (0.5 nm) is much smaller than the light wavelength, the accumulated phase mismatch normal to the film plane is negligible and the requirement of a matched wavevector normal
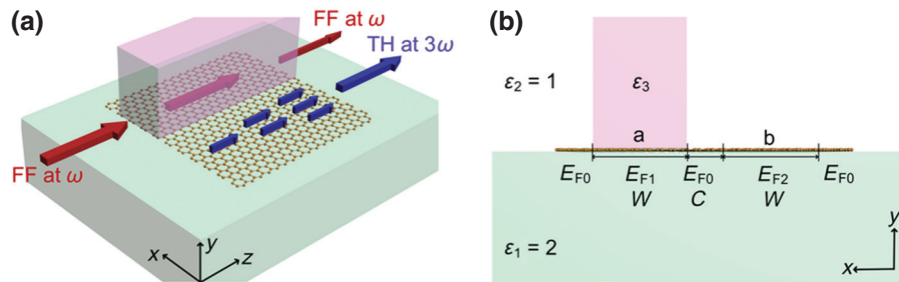

FIG. 1. The configuration of the graphene plasmonic coupler. (a) 3D schematic illustration. FF wave at a frequency of ω (red arrow) illuminating from the left-side nanoribbon is converted to a TH wave at a frequency of 3ω (blue arrow) in the right side. (b) 2D structure consisting of graphene nanoribbons with different doping levels sandwiched between dielectric media with relative permittivities of ϵ_1, ϵ_2, and ϵ_3. The corresponding chemical doping levels are E_{F0}, E_{F1}, and E_{F2}. $W = 8$ nm, $C = 2$ nm, and $E_{F0} = 1$ eV are fixed.

to the film is unnecessary. For propagating THG along the graphene film, perfect phase matching is essential to ensure the continuous increment of the generated harmonic power. The Fermi levels of the two graphene nanoribbons are set to be $E_{F1} = E_{F2} = 0.5$ eV at first. The FF wavelength is fixed to be $\lambda_1 = 6\,\mu$m during the calculation. Quantitative analysis of the phase-matching-assisted THG is presented in Fig. 2. The excited graphene plasmons provide a strongly localized and highly enhanced electromagnetic field. Ideally, we would like to use fundamental modes for both the FF and the TH waves, simply because of the high field enhancement. However, the dramatically localized field impairs pump-harmonic spatial overlap due to the lack of an evanescent mode component. It hence needs to equilibrate the field enhancement and mode localization to boost the pump-harmonic spatial overlap, and therefore, permit efficient THG. We thus examine three different PMC pairs with different guided-mode orders [two fundamental (0th) modes pair, first-order (1st) FF and 0th TH modes pair, and 0th FF and 1st TH modes pair].

The electromagnetic field profiles of the plasmonic modes in Fig. 2 emphasize the high level of nanoscale

localization. As shown in Figs. 2(a), 2(b), 2(d), 2(e), 2(g) and 2(h), the higher-order mode possesses lower intensity enhancement and a larger evanescent mode component. Figures 2(c), 2(f), and 2(i) depict the effective mode index at FF and TH waves and the corresponding THG conversion efficiency as a function of ϵ_3. The effective mode index tendencies reflect the achievability of PMC for different FF and TH modes pairs. The trade-off between the field enhancement and the evanescent mode component for FF and TH waves results in a larger pump-harmonic spatial overlap and a higher corresponding THG efficiency for the 0th FF and 0th TH modes pair as shown in Fig. 2(c). We study the mode-order effect here to emphasize modulating the coupling strength (determined by the pump-harmonic spatial overlap) between the FF and TH modes by controlling the guided mode order. Concurrently, different higher-order modes can phase match the pump wave to the third-harmonic wave, although most of them are unavailable for THG due to the small-field enhancement and the poor pump-harmonic spatial overlap. Figures 2(f) and 2(i) reveal that the THG efficiencies of the 1st TH and 0th FF PMC pair and the 0th FF and 1st TH PMC pair exceed
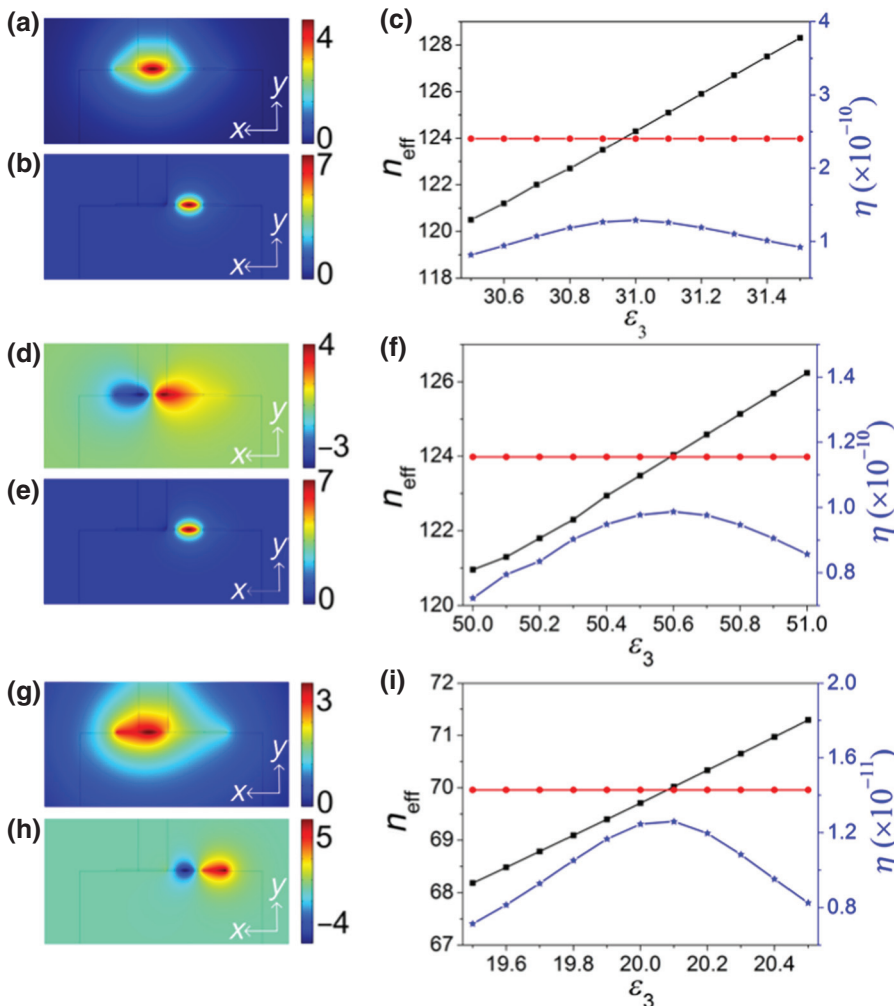

FIG. 2. THG assisted by PMC with stimulated plasmons producing high electric field enhancement. Electric field profiles of E_z in the x-y plane under PMC pairs between (a) 0th FF and (b) 0th TH modes, (d) 1st FF and (e) 0th TH modes, and (g) 0th FF and (h) 1st TH modes. (c),(f),(i) Effective mode index (n_{eff}) at FF and TH and the THG conversion efficiency (η) for the corresponding three PMC pairs as a function of the dielectric permittivity ϵ_3. Black: FF mode, red: TH mode, and blue: conversion efficiency.
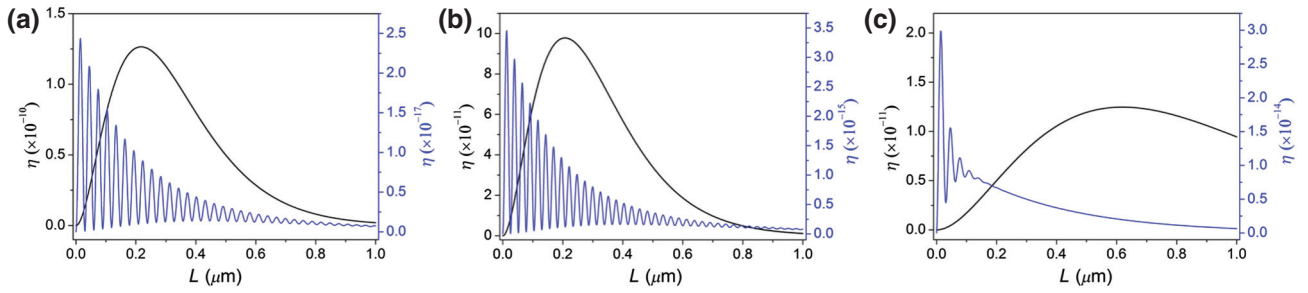
FIG. 3. THG conversion efficiency over the propagation distance under PMC (black, left y axis) and non-PMC (blue, right *y* axis) conditions for (a) 0th FF and 0th TH modes pair, (b) 1st FF and 0th TH modes pair, and (c) 0th FF and 1st TH modes pair.

three orders of magnitude compared to the value in free-standing graphene ($\eta = 1.9 \times 10^{-14}$, calculated with light normally incident on the extended graphene film). A relatively noticeable increment of 10^4-fold is achieved for the PMC pair between 0th FF and 0th TH, where the conversion efficiency goes up to 1.265×10^{-10}. The three different PMC pairs produce identical results, showing that PMC can greatly enhance the THG strength. Carefully controlling the guided mode order is necessary as well to optimize the third-order nonlinear process.

PMC represents the ideal state where the FF power continuously transfers to the TH power. Figure 3 depicts the THG conversion efficiency over the propagation distance along the graphene plasmonic coupler. For non-PMC conditions, the ϵ_3 value for the different mode pairs is set to be half of the corresponding value at which the PMC is satisfied. Due to the phase mismatch, the build-up continuity of the TH power is limited to the coherence length, over which a phase difference of π accumulates between the FF and the TH waves. With PMC, the FF and TH waves can propagate with the same phase velocity, and accordingly, the TH signal energy is able to accumulate

continuously along its propagation as depicted by the black lines in Fig. 3. More than two (four) orders of magnitude improvement in the conversion efficiency is achieved for the 1st FF and 0th TH modes pair (0th FF and 1st TH modes pair), and over six orders of magnitude improvement for the 0th FF and 0th TH modes pair. This is due to the greatly increased effective nonlinear interaction length under PMC and the light energy from the pump wave is continuously transformed to the signal's third harmonic. The peak THG conversion efficiency is caused by the interplay between the propagation loss and the converted third-harmonic power (per unit length). The intrinsic graphene layer is considered as the primary source of loss due to the interband absorption and intraband transition. No Landau damping is considered. The plasmon damping induced by the interband excitation can be greatly suppressed when the Fermi energy is larger than the plasmon energy. We only consider the loss due to intraband transitions during the calculation.

In addition to PMC, another nontrivial aspect of the graphene plasmonic coupler is the peak graphene $\chi^{(3)}$. An analytical formalism of $\chi^{(3)}$ for doped graphene
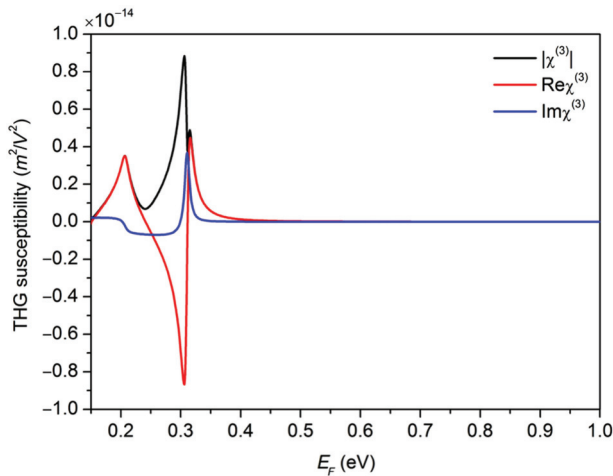

FIG. 4. Total (black line), real (Re, red line) and imaginary (Im, blue line) parts of the graphene $\chi^{(3)}$ at $6\,\mu$m under different doping levels.
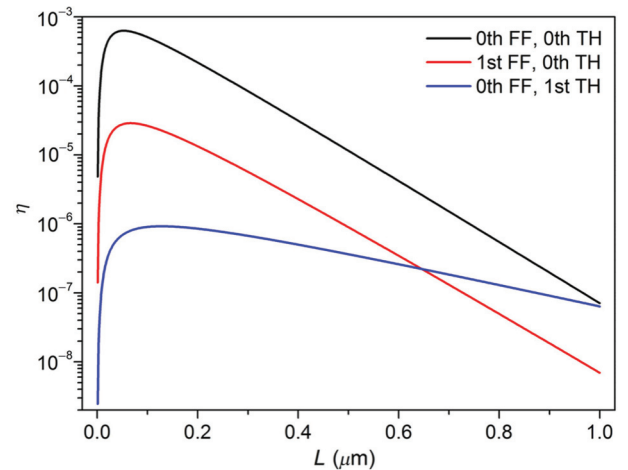

FIG. 5. THG conversion efficiency along the propagation distance for 0th FF and 0th TH (black line), 1st FF and 0th TH (red line), and 0th FF and 1st TH (blue line) PMC pairs.
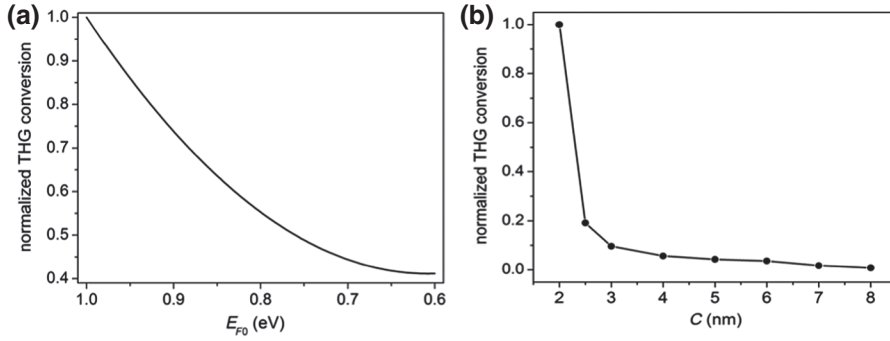
FIG. 6. Normalized THG conversion efficiency of left-peak $\chi^{(3)}$ case at PMC for 0th FF and 0th TH as a function of (a) background graphene Fermi level E_{F0} with fixed $C = 2$ nm, and (b) separation C at $E_{F0} = 1$ eV.

based on the Genkin-Mednis nonlinear conductivity theory has been reported [24], indicating the dependence of the graphene $\chi^{(3)}$ magnitude on the carrier concentration and the working frequency (see Appendix B). Graphene possesses a resonant peak in $\chi^{(3)}$ when the light frequency equals two-thirds of the Fermi level. Peak graphene $\chi^{(3)}$ can be pursued when the Fermi level is set to be 0.31 eV for the FF wavelength fixed at 6 μm. We study three peak $\chi^{(3)}$ cases in the plasmonic coupler for efficient THG conversion: left-peak $\chi^{(3)}$ case ($E_{F1} = 0.31$ eV, $E_{F2} = 0.5$ eV), right-peak $\chi^{(3)}$ case ($E_{F1} = 0.5$ eV, $E_{F2} = 0.4$ eV), and two-peak $\chi^{(3)}$ case ($E_{F1} = 0.31$ eV, $E_{F2} = 0.4$ eV). The real and imaginary $\chi^{(3)}$ values with different graphene doping levels are depicted in Fig. 4. For the right-peak and two-peak $\chi^{(3)}$ cases, the Fermi level of nanoribbon b is set to be 0.4 eV, because when E_{F2} is set to be 0.31 eV, it becomes difficult to stimulate TH plasmons in nanoribbon b and it is unlikely to realize PMC by only tuning ϵ_3. For the left-peak $\chi^{(3)}$ case, THG efficiency at a level of 10^{-4} is achieved between the 0th FF and the 0th TH, as shown in Fig. 5. Compared with the pure PMC conditions in Fig. 2, E_{F2} and the surrounding dielectric of nanoribbon b are kept unchanged. On the other hand, the electric field enhancement of the FF wave is further increased for different PMC pairs because the lower Fermi level value corresponds to a smaller wavevector for graphene plasmons. Due to the trade-off between field enhancement and mode localization, the pump-harmonic-mode overlap reaches its maximum value under two fundamental modes pair. The obtained highest conversion efficiency of 6.3051×10^{-4} is more than 10 orders of magnitude larger than that in a freestanding monolayer graphene. THG efficiencies of 2.8787×10^{-5} and 9.2154×10^{-7} are achieved for the other two PMC pairs. These smaller THG efficiencies result from the smaller FF and TH field enhancements.

For the right-peak $\chi^{(3)}$ case (see details in Fig. S1 [33]), the highest conversion of 2.1576×10^{-10} is provided by the 1st FF and 0th TH PMC pair. Even though nanoribbon b is the main interaction nonlinear matter and its $\chi^{(3)}$ is larger compared with the left-peak $\chi^{(3)}$ case, it is still difficult to achieve a higher THG efficiency. The electric field distribution for the three different PMC pairs shows reduced evanescent mode components, which leads to very

small pump-harmonic spatial overlap. For the two-peak $\chi^{(3)}$ case (see details in Fig. S2 [33]), the plasmonic coupler offers higher nonlinearity, while it suffers from a large propagating loss and strong nonlinear phase modulations. The nonlinear interaction length is reduced to less than 20 nm. Although the pump-harmonic spatial overlap is noticeable in this case, the generated TH power drops too quickly to obtain an efficient THG.

Considering the practical availability, we provide the background Fermi level E_{F0} and the separation C dependences of the THG conversion at PMC in Fig. 6. As shown in Fig. 6(a), although a 60% decrement of the THG efficiency is induced when decreasing the background Fermi level to 0.6 eV, the corresponding conversion efficiency is still over nine orders of magnitude larger than that from bare graphene. Further decreasing the background Fermi level to be less than 0.6 eV makes it difficult to obtain PMC by only tuning the permittivity of the top cladded layer. Since PMC guarantees the continuous transformation of the pump power to the third-harmonic power, we recommend doping the background graphene to 0.6 eV or larger. From Fig. 6(b), the THG efficiency at a separation of 8 nm is decreased to 0.82% of that from the coupler at a separation of 2 nm due to the weakening of the coupling strength. Even so, the THG efficiency is seven orders of magnitude higher than that from a bare monolayer graphene. Therefore, our proposed graphene plasmonic coupler is suitable for efficient THG in practical applications. Note that the quantum size and nonlocal effects as well as the temperature dependence of the graphene conductivity are not included in our current calculations. These effects may change the quantitative values of the results we obtain, while the idea of using phase matching and peak third-order nonlinear susceptibility still remains valid. Further investigations of the quantum effects and temperature dependence are beyond the scope of this work. We will leave these investigations to our future study.

IV. CONCLUSION

In conclusion, the combination of PMC and peak third-order nonlinear susceptibility provided by the graphene plasmonic coupler leads to a significantly enhanced THG.

A THG efficiency as high as 6.3051×10^{-4} is achieved, possessing more than 10 orders of magnitude higher than that of a bare monolayer graphene. The plasmonic modes at FF and TH modes provide high field enhancement, and the PMC ensures the continuous transformation of the FF power to the TH power. The peak $\chi^{(3)}$ of doped graphene offers intense nonlinearity and thereby a remarkable nonlinear response. Our calculation represents a theoretical evidence of extraordinary THG from a nanoscale graphene plasmonic coupler structure at the midinfrared regime, which ensures further exploration of tunable subwavelength nonlinear coherent sources and ultra-compact signal processing in midinfrared and terahertz spectral regimes.

ACKNOWLEDGMENTS

APPENDIX A: COMSOL SIMULATION

Finite-element-method calculations for fundamental- and third-harmonic mode profiles and their mode indices based on commercial COMSOL multiphysics are performed. Graphene is modeled as a thin layer with a thickness of 0.5 nm by a dielectric function of $1 + i\sigma(\omega)/(\omega\varepsilon_0 t_g)$, where $\sigma(\omega)$ is the linear graphene surface conductivity described by the Kubo formula, ω is the light frequency, and t_g is the graphene layer thickness (0.5 nm). Drude-like form conductivity of $\sigma(\omega) = ie^2 E_F/[\pi\hbar^2(\omega + i\tau^{-1})]$, where $-e$ is the electron charge, $\hbar$ is the reduced Planck's constant, and τ is the carrier relaxation time is used due to the high doping level. We set the carrier relaxation time to $\tau = 0.1$ ps during the calculation according to the measured, impurity limited dc mobility $\mu \approx 10\,000\,\text{cm}^2\,\text{V}^{-1}\,\text{s}^{-1}$ [30–32]. A larger relaxation time (i.e., lower degrees of propagation loss) can be used to further enhance the harmonic generation efficiency.

APPENDIX B: PEAK THIRD-ORDER NONLINEAR SUSCEPTIBILIY OF GRAPHENE

The static limit ($\omega \to 0$) of the THG susceptibility of graphene can be described as $\chi^{(3)}(0) = 1.65$ $e^2(h\upsilon_F)^2/[\pi\varepsilon_0 d_g(2E_F)^5]$ [24], where $\upsilon_F = 10^6\,\text{m}\,\text{s}^{-1}$ is the graphene Fermi velocity, ϵ_0 is the vacuum permittivity, and $d_g = 0.5$ nm is the effective thickness of the graphene layer.

For a nonzero ω, $\chi^{(3)}$ of graphene can be obtained by

$$\chi^{(3)}(-3\omega : \omega, \omega, \omega)$$
$$= \chi^{(3)}(0) \left\{ \begin{array}{l} \left[\dfrac{10}{11}F^1_{\text{inter}}(Z) + \dfrac{40}{33}F^1_{\text{comb}}(Z) \right] \\ +i\delta \left[\dfrac{10}{11}F^2_{\text{inter}}(Z) + \dfrac{40}{33}F^2_{\text{comb}}(Z) \right] \end{array} \right\}.$$

The dimensionless functions $F_{\text{inter}}(Z)$ and $F_{\text{comb}}(Z)$ are used to describe the Fermi level and frequency dependence of the nonlinear optical process. $Z = \hbar\omega/E_F$ and $\delta = \hbar\Gamma/E_F$ represent the photon energy and the broadening parameter normalized to the Fermi level. Table SI [33] shows the values of all parameters involved to calculate $\chi^{(3)}(-3\omega; \omega, \omega, \omega)$ at different Fermi levels.

[1] M. Kauranen and A. V. Zayats, Nonlinear plasmonics, Nat. Photonics **6**, 737 (2012).

[2] C. Clavero, Plasmon-induced hot-electron generation at nanoparticle/metaloxide interfaces for photovoltaic and photocatalytic devices, Nat. Photonics **8**, 95 (2014).

[3] V. N. Konopsky, E. V. Alieva1, S. Y. Alyatkin, A. A. Melnikov, S. V. Chekalin, and V. M. Agranovich, Phase-matched third-harmonic generation via doubly resonant optical surface modes in 1D photonic crystals, Light: Sci. Appl. **5**, e16168 (2016).

[4] T. Wu, P. P. Shum, X. Shao, T. Huang, and Y. Sun, Third harmonic generation from mid-IR to near-IR regions in a phase-matched silicon-silicon nanocrystal hybrid plasmonic waveguide, Opt. Express **22**, 24367 (2014).

[5] T. Wu, P. P. Shum, Y. Sun, X. Shao, and T. Huang, Study on the crucial conditions for efficient third harmonic generation using a metal-hybrid-metal plasmonic slot waveguide, Opt. Express **23**, 253 (2015).

[6] G. Li, S. Chen, N. Pholchai, B. Reineke, P. W. H. Wong, E. Y. B. Pun, K. W. Cheah, T. Zentgraf, and S. Zhang, Continuous control of the nonlinearity phase for harmonic generations, Nat. Mater. **14**, 607 (2015).

[7] B. Metzger, M. Hentschel, T. Schumacher, M. Lippitz, X. Ye, C. B. Murray, B. Knabe, K. Buse, and H. Giessen, Doubling the efficiency of third harmonic generation by positioning ITO nanocrystals into the hot-spot of plasmonic gap-antennas, Nano Lett. **14**, 2867 (2014).

[8] A. Paul, R. A. Bartels, R. Tobey, H. Green, S. Weiman, I. P. Christov, M. M. Murnane, H. C. Kapteyn, and S. Backus, Quasi-phase-matched generation of coherent extreme-ultraviolet light, Nature **421**, 51 (2003).

[9] T. Wu, P. P. Shum, Y. Sun, T. Huang, and L. Wei, Third harmonic generation with the effect of nonlinear loss, J. Lightwave Techno. **34**, 1274 (2015).

[10] M. S. Nezami, D. Yoo, G. Hajisalem, S. Oh, and R. Gordon, Gap plasmon enhanced metasurface third-harmonic generation in transmission geometry, ACS Photonics **3**, 1461 (2016).

[11] F. J. García de Abajo, Graphene plasmonics: Challenges and opportunities, ACS Photonics **1**, 135 (2014).

[12] L. Ju, B. Geng, J. Horng, C. Girit, M. Martin, Z. Hao, H. A. Bechtel, X. Liang, A. Zettl, Y. R. Shen, and F. Wang, Graphene plasmonics for tunable terahertz metamaterials, Nat. Nanotechnol. **6,** 630 (2010).

[13] M. Gullans, D. E. Chang, F. H. L. Koppens, F. J. G. García de Abajo, and M. D. Lukin, Single-Photon Nonlinear Optics with Graphene Plasmons, Phys. Rev. Lett. **111,** 247401 (2013).

[14] S. A. Mikhailov, Theory of the giant plasmon-enhanced second-harmonic generation in graphene and semiconductor two-dimensional electron systems, Phys. Rev. B **84,** 045432 (2011).

[15] Z. Fei, A. S. Rodin, G. O. Andreev, W. Bao, A. S. McLeod, M. Wagner, L. M. Zhang, Z. Zhao, M. Thiemens, G. Dominguez, M. M. Fogler, A. H. Castro Neto, C. N. Lau, F. Keilmann, and D. N. Basov, Gate-tuning of graphene plasmons revealed by infrared nanoimaging, Nature **487,** 82 (2012).

[16] K. V. Sreekanth, S. Zeng, J. Shang, K. T. Yong, and T. Yu, Excitation of surface electromagnetic waves in a graphene-based Bragg grating, Sci. Rep. **2,** 737 (2012).

[17] N. Kumar, J. Kumar, C. Genstenkorn, R. Wang, H. Y. Chiu, A. L. Smirl, and H. Zhao, Third harmonic generation in graphene and few-layer graphite films, Phys. Rev. B **87,** 121406 (2013).

[18] S. Y. Hong, J. I. Dadap, N. Petrone, P. C. Yeh, J. Hone, and R. M. Osgood, Jr., Optical Third-Harmonic Generation in Graphene, Phys. Rev. X **3,** 021014 (2013).

[19] J. L. Cheng, N. Vermeulen, and J. E. Sipe, Third order optical nonlinearity of graphene, New J. Phys. **16,** 053014 (2014).

[20] J. L. Cheng, N. Vermeulen, and J. E. Sipe, Third-order nonlinearity of graphene: Effects of phenomenological relaxation and finite temperature, Phys. Rev. B **91,** 235320 (2015).

[21] S. A. Mikhailov, Quantum theory of the third-order nonlinear electrodynamic effects of graphene, Phys. Rev. B **93,** 085403 (2016).

[22] E. Hendry, P. J. Hale, J. Moger, A. K. Savchenko, and S. A. Mikhailov, Coherent Nonlinear Ooptical Response of Graphene, Phys. Rev. Lett. **105,** 097401 (2010).

[23] T. Gu, N. Petrone, J. F. McMillan, A. van der Zande, M. Yu, G. Q. Lo, D. L. Kwong, J. Hone, and C. W. Wong, Regenerative oscillation and four-wave mixing in graphene optoelectronics, Nat. Photonics **6,** 554 (2012).

[24] V. A. Margulis, E. E. Muryumin, and E. A. Gaiduk, Frequency dependence of optical third-harmonic generation from doped graphene, Phys. Lett. A **380,** 304 (2016).

[25] H. A. Haus and W. P. Huang, Coupled-mode theory, Proc. IEEE **79,** 1505 (1991).

[26] R. W. Boyd, *Nonlinear Optics* (Academic Press, Boston, 2003).

[27] V. P. Gusynin, S. G. Sharapov, and J. P. Carbotte, Unusual Microwave Response of Dirac Quasiparticles in Graphene, Phys. Rev. Lett. **96,** 256802 (2006).

[28] N. M. R. Peres, F. Guinea, and A. H. C. Neto, Electronic properties of disordered two-dimensional carbon, Phys. Rev. B **73,** 125411 (2006).

[29] M. Jablan, H. Buljan, and M. Soljačić, Plasmonics in graphene at infrared frequencies, Phys. Rev. B **80,** 245435 (2009).

[30] K. S. Novoselov, A. K. Geim, S. V. Morozov, D. Jiang, Y. Zhang, S. V. Dubonos, I. V. Grigorieva, and A. A. Firsov, Electric field effect in atomically thin carbon films, Science **306,** 666 (2004).

[31] K. S. Novoselov, A. K. Geim, S. V. Morozov, D. Jiang, M. I. Katsnelson, I. V. Grigorieva, S. V. Dubonos, and A. A. Firsov, Two-dimensional gas of massless Dirac fermions in graphene, Nature **438,** 197 (2005).

[32] F. H. Koppens, D. E. Chang, and F. J. Garcia de Abajo, Graphene plasmonics: A platform for strong light–matter interactions, Nano Lett. **11,** 3370 (2011).

[33] See the Supplemental Material at http://link.aps.org/supplemental/10.1103/PhysRevApplied.11.014049 for parameters involved in the calculation of the $\chi^{(3)}$ of graphene at different Fermi levels, and the electric field profiles in the x-y plane under different PMC pairs for the right-peak $\chi^{(3)}$ and two-peak $\chi^{(3)}$ cases.